Effects of nanoscale film thickness on apparent stiffness of and cell-mediated strains in polymers

by

Binu K Oommen

Submitted to the Department of Materials Science and Engineering
in partial fulfillment of the requirements for the degree of

Master of Science in Materials Science and Engineering

at the

MASSACHUSETTS INSTITUTE OF TECHNOLOGY

September 2006

Author .....
Department of Materials Science and Engineering
April 24, 2006

Certified by .....
Krystyn J. Van Vliet
Lord Foundation Assistant Professor
Thesis Supervisor

Accepted by .....
Samuel M. Allen
POSCO Professor of Physical Metallurgy
Chair, Departmental Committee on Graduate Students

Effects of nanoscale film thickness on apparent stiffness of and cell-mediated strains in polymers

by

Binu K Oommen

Submitted to the Department of Materials Science and Engineering
on April 24, 2006, in partial fulfillment of the
requirements for the degree of
Master of Science in Materials Science and Engineering

Abstract

The mechanical properties of compliant materials such as polymeric films and biological membranes that are of nanoscale in thickness are increasingly extracted from scanning probe microscope-enabled nanoindentation. These films are applied in various fields that require multiaxial loading conditions. The Hertzian contact models developed for linear elastic materials of semi-infinite thickness fail to accurately predict the elastic modulus E for these compliant materials. This makes it necessary to understand the evolution of stress and strain fields of these nanoscale structures. In this thesis we employ computational simulations that are based on experimental parameters for contact based analysis of compliant polymer thin films, to decouple the effect of thickness and angle of indentation on calculated mechanical properties. Traction applied by living cells to these compliant films are studied in detail. We thus identify the range of strains and material thickness for which contact models could be used to accurately predict the elastic stiffness of these polymeric films of nanoscale ($<$ 100 nm) thickness using scanning probe microscope-enabled experiments, and the volumes over which adhered cells deform these films. The key results of this thesis enable accurate experimental analysis of polymeric thin film elastic properties, and design of synthetic polymeric substrata that will dominate the mechanical environment of adhered cells.

Thesis Supervisor: Krystyn J. Van Vliet
Title: Lord Foundation Assistant Professor

Acknowledgments

This thesis is a result of several semesters of work whereby I have been accompanied and supported by many people whom I would like to thank and express my sincere gratitude.

First of all I would like to thank my advisor Prof. Krystyn van Vliet, whose consistent support, care and enthusiasm towards my research, bears fruit in the form of this thesis. She devoted many hours of her quality time in bringing out the best out of me and has all along made a deep impression on me. Besides being an excellent advisor, she is as close as a relative and a good friend to me and my family.

I have been blessed with a wonderful group, the vvgroup. The group always gave a feeling of being at home in the work environment. The group also actively contributed to the development of this work, through fruitful discussions and interactions that helped me shape this work. I would also like to thank all my friends who helped me in different ways at different times in completing this thesis.

This work was supported primarily by the MRSEC Program of National Science Foundation under award number DMR 02-13282. I am also grateful to the department of materials science and engineering, for providing me with the excellent work environment during the course of this work.

The prime motivation and support for my work, comes from my family, especially my father and mother, who has been a source of inspiration for me through out my life. My wife, Sheba has been the strength and support for me.

Contents

List of Figures

Chapter 1

Introduction

Polymeric films of nanometer-scale thickness such as polyelectrolyte multilayers (PEMs) and poly(dimethyl siloxane) (PDMS) are increasingly finding application in a wide range of scientific fields ranging from bioengineering via synthetic cell substrata [14, 20] to tunable Bragg reflectors [9]. The mechanical properties such as (visco)elastic moduli, play a very important role in defining the applications towards which these nano-scale films can be applied. These properties are not expected to vary with length scale but can be influenced through external artifacts of measurement. In the context of biological applications, the mechanical properties of these films affect cell functions ranging from mitosis to proliferation to programmed cell death [40, 13, 37]. The goal of this thesis is to model the effects of finite thickness and contact conditions on the accurate estimation of (visco)elastic stiffness for polymeric films including nanoscale substrata and nanoscale cells. These contact conditions include pure normal loading (indentation) and pure shear loading (cell focal adhesion traction).

One of the techniques that can test the mechanical properties of these materials to nanoscale precision is scanning probe microscopy (SPM)enabled indentation. The most common elastic contact formulations such as Hertzian [17] theory are used to extract the mechanical properties of these materials, and are based on the assumption that the material is continuous, homogeneous, elastic and relatively large in geometry such that the external boundary conditions do not influence the estimation of a given property. However, care must be taken in implementing these models to polymeric

films, which are usually non-linear elastic materials exhibiting time-dependent responses, such that external boundary conditions can significantly influence calculated properties. One goal of this thesis is to decouple the geometric and mechanical properties of viscoelastic thin films, and show how each independently affects the stress and strain fields within the film.

Because of the increasing application of SPMs to evaluate the mechanical properties via analysis of force-displacement responses, it is important to also evaluate the experimental errors which could influence the calculated properties. One of these errors is the inclination of the SPM cantilever with respect to the sample surface. The tilt of the cantilever is necessary to ensure that the free end of the cantilever touches the sample first. However this tilt influences the effective material stiffness(which is a function of cantilever spring constant and tilt), inducing erroneous measurement results [25]. Through systematic variation of cantilever angle and sample thickness, the effect of varying each parameter is studied in detail.

In order to understand the geometric and material effects during mechanical testing or application of external loading situations, it is important to understand how these stress and strain fields evolve. One such example is the way in which cells respond when the geometry and stiffness of the substrate to which they are attached are varied[40]. The chemomechanical environment of living cells has been shown to be influenced by these changes in external environment [24]. The influence of constant stress which is exerted by a cell onto a polymeric substrate is evaluated as a function of the polymer elastic modulus and thickness,as well as the number of cellular focal adhesions (FAs).

Elastic modulus maps enabled by SPMs can be used to evaluate cell stiffness during various processes such as cell migration, or over different regions of the cell [13, 5]. Just as in the analysis of the film mechanical properties, the formulations from contact mechanics for deformable bodies are used in conjunction with force-displacement responses collected from SPMs to estimate the elastic modulii at individual points on the cell surface [13, 51, 21]. The concluding part of this thesis implements this tool for evaluting cell stiffness over the cell surface.

Chapter 2 provides a brief literature review of mechanical modeling and characterization of polymeric films and cells. Chapter 3 details the computational modeling pertinent to each study, and Chapter 4 presents Results and Discussion of these decoupled geometric and contact parameters for (bio)polymeric thin film mechanical analysis. Chapter 5 enumerates the conclusions resulting from this study and discusses briefly possible ideas which originated during this thesis, that will be studied as future work.

Chapter 2

Literature Review

Rapid advances in technology and process development techniques have made it possible to see, feel and apply nanometer scale objects in a wide variety applications in science. This section discusses the advances made in characterization techniques for mechanical properties of nanoscale polymer films and how these are applied to better understand the internal characteristics of these films under various multiaxial loading conditions. The progress made in the field of cell mechanics in understanding the effects of loads (traction by cells) on these synthetic substrata are reviewed. Also reviewed are the research studies that combine cell mechanics with substrate properties in creating the maps for local mechanical properties.

2.1 Mechanical characterization of nano-scale films

Mechanical properties such as elastic moduli are very important parameters that need to be measured accurately in order to apply these polymeric films in various fields of science. For thin films and polymers, estimated moduli are significantly affected by external boundary conditions and experimental conditions. In the following sections, the advances in understanding how these external parameters influence the calculated modulii values are discussed.

2.1.1 Effects of film thickness on estimated mechanical properties

Mechanical properties such as elastic modulus E are measured from the load-deflection $(P - h)$ data extracted from nanoindentation. Studies in metallic and ceramic thin films have shown that E is very strongly influenced by the thickness of the thin film, and that calculated film properties differ very much from the bulk materials due to this external artifact. The way in which contact-induced stresses are transferred to the film/substrate interface and to the substrate itself very strongly influences the estimated mechanical properties [32, 13]. The influence of the underlying substrate on calculated mechanical properties has been addressed by several investigators for conical indenter geometries [38, 11, 4, 46]. In this case, the contact stresses decay sharply with distance from the indenter. This means that the mechanical properties of the sample can be measured accurately if these contact stresses are totally confined inside the film. Hence to capture only the response of the film, it is common to limit the indentation depth h_{max} to less than 10% of the film thickness t. This is a purely empirical estimate vary as a function of elastic and plastic mismatch between the film and substrate [36]. These empirical relations may not hold when the sample property exhibits non-linear elasticity or viscoelasticity.

The inherent geometric nonlinearity of multiaxial contact makes it difficult to obtain a closed form solution for contact of mechanically compliant samples that are of finite thickness. The failure of Hertzian contact mechanics to estimate E from the loading portion of the $(P - h)$ indentation response for samples that are compliant and of finite thickness has been addressed by others [6]. Dimitriadis et al. developed a modified model which takes into account the effect of film thickness variation by deriving the Green's function for a sample of finite thickness bonded to the substrate. This model showed that for a given spherical indenter probe radius, there exists a range of sample thickness t and indentation depth h. The fundamental assumption in these modeling techniques are that the material is a linear elastic solid, with the maximum nominal contact strains not exceeding 10% or $h \leq 0.1t$. These models

are based on the early work of Chen et al., which addressed the problem of stresses and strain fields in mulitlayer media that is well-adhered to the substrate [52, 44]. The Poisson's ratio ν has been shown to influence E differently compared to models developed by Dimitriadis et al., when the finite thickness effect was considered [21]. More conservative corrections for finite thickness were added through different models, which also included the constraint of poorly adhered films. These models estimated the complex elastic modulus and ν of mammalian cells via SPM-enabled nanoindentation. Although the modeling assumptions and approaches adopted for developing these models differ, they all address the error in accurate determination of E via contact-based measurements on thin, compliant polymer films.

For the specific case of polyacrylamide hydrogels of thickness $t = 5$ μm and for a maximum indentation depth of $h_{max} = 3$ μm, it has been shown that the experimental $P - h$ responses agree well with the thickness-corrected Hertzian elastic cone model proposed by Dimitriadis et al. In contrast, studies have shown that E for PEM of μm-scale thickness is a function of t when calculated from SPM-enabled spherical nanoindentation of hydrated, nanoscale PEM films even when this thickness correction is applied to the linear elastic Hertzian elastic sphere model [37]. Finally it has also been demonstrated that E calculated from SPM-enabled spherical nanoindentation of hydrated, nanoscale PEM films with t $<$ 200 nm, agrees well with the elastic moduli calculated from other independent experimental techniques and also by other researchers for similar PEMs [40] even in the absence of thickness correction factors.

An important question emerging out of these contrasting results is whether the E of polymer films that are of nanoscale in thickness and measured via SPM-enabled indentation are intrinsic properties of the material, or external artifacts due to combinations of finite thickness, large strains, and the inherent nonlinear elasticity of the polymeric material.This becomes a critical issue when these polymeric films are used for mechanics-critical applications that range from biological substrata to low-dielectric constant films in integrated circuits. Computational techniques such as finite element analysis (FEA) can be used to analyze the mechanics of deformations of these thin films which exhibit stress behaviors that are not confined inside the film

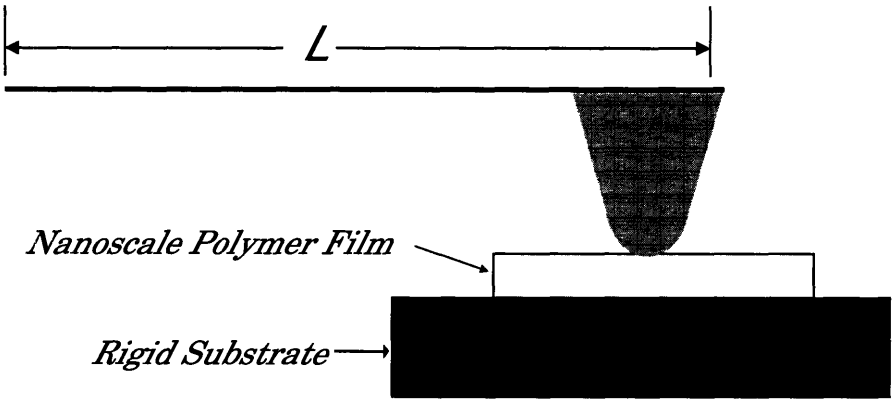

Figure 2-1: Schematic of indentation setup in Hertzian formulation.

geometry. The stress evolution beyond the elastic limit has been simulated via FEA for thin films made of layered metal (titanium/aluminum) [22]. In this study, we simulate the nanoindentation of polymeric thin films using spherical indenters to analyze the deformation field behavior which exists as a function of stress, film thickness, and material constitutive model. Even though FEA are continuum based simulations that are independent of length scale, this study provides important information about the changes in stress and strain fields during nanoindentation when the thickness of these films are reduced to the nanometer scale in thickness.

2.1.2 Effects of indenter angle on mechanical properties

The objective in section 2.1.1 was to understand how the geometric parameter such as thickness of the sample influences E. This section discusses another critical question: Does the angle of indentation influence the estimation of mechanical properties, especially for a case where thickness of the sample is on the order of nanometers? Figure 2-1 shows the schematic for which the Hertzian formulation [17] is used. Here the indentation is normal to the sample. However in conventional SPMs the indentation is imposed at an angle θ as shown in figure 2-2. This tilt angle is usually around 12° to 15° in conventional SPMs. The Hertzian formulations described in the next chapter do not account for this tilt during indentation.

Even though tilt of the cantilever is known to affect the properties being measured,

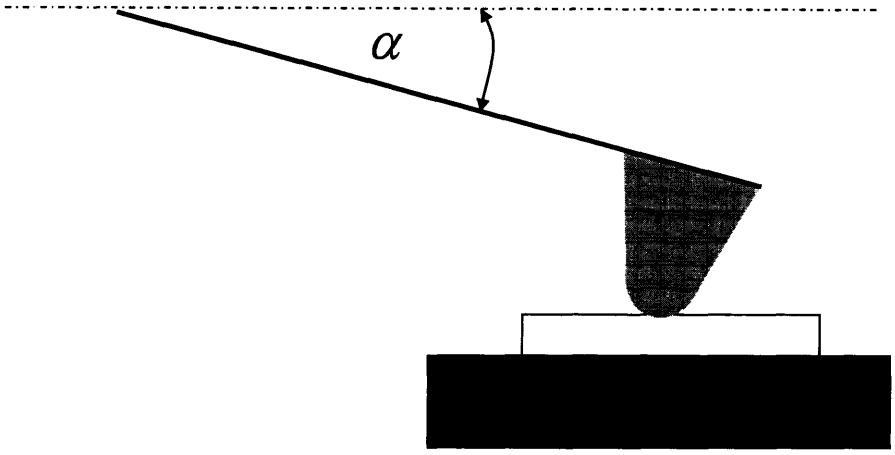

Figure 2-2: Schematic of cantilever tilted by an angle θ with respect to the horizontal surface.

most of the estimations of mechanical properties are based on the assumption that the indenter is oriented normal to the sample geometry during indentation [15, 12]. In experiments such as studying adhesion of a particle (for example: when studied in context of flow behavior of powders and granular media), the tilt of the cantilever can have a significant influence on the absolute values of adhesion forces measured [25, 27].Effective cantilever stiffness $K_{effective}$ is increased by 10% - 20% as the tilt of the cantilever increases [25], and is given by

$$K_{effective} = \frac{K}{cos^2\theta[1 - 2D\tan\frac{\theta}{L}]} \tag{2.1}$$

where K is the stiffness of the cantilever, D is the diameter of the tip, L is the length of the cantilever and θ is the tilt of the cantilever with respect to the sample plane [25].

When the cantilever is tilted, the force that is induced on the sample is not directed perpendicular to the surface. The force components are split into one that is directed parallel to the cantilever length and another directed perpendicular to the cantilever length. The force that is directed parallel to the cantilever causes a torque, which induces only a small change in deflection but a large change in the inclination of the cantilever at the end [25].

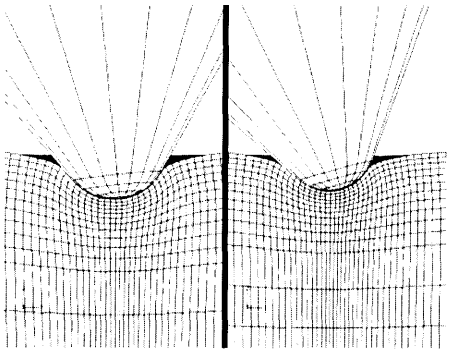

Figure 2-3: Change in contact area as angle of indentation changes from 6° to 15° for an indentation depth of 25 nm and D = 25 nm.

One of the parameters which changes with indentation depth is the contact area A, which is invariant with θ for a sphere, but not for a sphere-tipped cone. The calculations which are used to extract E are based on the assumption that the indenter geometry is spherical in shape, which is not always the case. As the angle of inclination changes, so does the contact geometry. A transition occurs from a spherical geometry to a conical one. This fact is shown in figure 2-3, for an indentation depth of 25 nm. It is seen that the geometry makes a transition from sphere (when θ= 6°)to conical (when θ= 15°). This increase in contact area is an external artifact caused due to the increase in tilt angle of the cantilever which affects the calculated mechanical properties such as stiffness.The reason for this is explained below.

In most SPMs, the optical lever technique is used for detecting the cantilever deflection. This means that the optical lever senses the cantilever deflection d and not the inclination, from which the force is inferred as $F = kd$, hence making the actual angle of inclination a critical parameter in property estimations. Correction factors which are based on the geometry of the indenter have been proposed by several researchers [25, 19]. The correction factor is defined as the ratio of inclination of a horizontal cantilever to the inclination of a tilted cantilever to which the same force is applied. For a cantilever with a tip of conical shape this factor is $cos^2\theta$(1-2$Dtan\theta/L$) while the correction factor for a tip of spherical shape is $cos^2\theta$(1-2$Rtan\theta/L$), where R and D are the indenter tip radius and the height of the cone respectively.

2.2 Effects of stresses exerted by focal adhesions on films of varying thickness

The direct application of these thin, nanoscale polymer films is as synthetic substrata for studying cellular function such as cell migration, cell adhesion, and cell differentiation. Among several topics, one area of interest is the interaction between cells and substrates through focal adhesions, which are activated during transduction of local mechanical forces that are rapidly converted into biological signals. Focal adhesions (FAs) are large, mulitprotein complexes that provide a link between the cytoskeleton and surrounding extracellular matrix [3]. The critical question we ask here is: How does traction, exerted by the cells through FAs, affect the evolution of stress and strain fields when the thickness and modulus of these films are varied?

Many researchers have studied cell functions over different types of substrates. These substrates varied in their shape from patterned substrates to deformable substrates embedded with chemically functionalized micro-beads [35, 24, 52, 28]. By using different synthesis techniques, E of these substrates are varied from the Pa to MPa range [28, 40]. These studies have shown that the cells feel the underlying substrate and actively respond to this change in local mechanical environment. The rigidity of these substrates can regulate the formation and maintenance of tissues [18], and the variation in mechanical properties of these substrates modulates the mechanotransduction pathways [16].

The traction exerted by stationary fibroblasts has been shown to be a constant value of 5 $nN/\mu m^2$ [1]. Recently it has been demonstrated for fibroblasts that the stresses exerted by these FAs increase exponentially when the area of FAs increases beyond 8 μm^2 [30]. These increases in traction have also been associated with an increase in smooth muscle actin in fibroblasts, which is a sign of increased intracellular tension. These mechanotransduction phenomena occurring inside FA depends on a balance between the local mechanical stress and specific biochemical signals [29].

The sensing mechanisms differ from cell type to cell type. Fibroblasts show strong adhesion and proliferation characteristics on substrates of very high elastic modulus,

while neurons grow best on more compliant substrates [50]. The fibroblasts showed no stress fibers on softer substrates [50]. The cellular traction also increases with increase in substrate E [30, 50]. Experiments have shown that the cells migrate preferentially towards stiffer substrates from more compliant ones [35]. The mechanism through which FA assemble, elongate and dissociate on application of external forces are not well understood. It is shown that the force level, force distribution, and character of anchoring of cells to the substrate all affect the FAs [47]. Studies on flexible silicone substrates using beads as markers have shown that the forces exerted by motile fibroblasts onto their extracellular matrix environment are highly localized [49].

The demonstration that cells can deform the underlying substrate, and that substrate modulus can in turn affect cell behavior, indicates a coupled relationship between cells and the extracellular environment [41]. As the above studies show, there is a great deal of experimental data available on the behavior of cells on deformable substrates, but very little information is available on how the stress fields within the substrates evolve when cellular traction is exerted. Understanding this evolution would help to determine the range over which cells sample their local mechanical environment, and how thick substrata must be to dominate the mechanical environment. This thesis addresses this question through computational modeling of the substrates as thin polymeric film.

2.3 Mechanical characterization of living cells through modulus mapping

SPMs can be used to measure the topography of materials and also the mechanical properties such as elastic modulii and viscoelastic modulii. To understand cellular physiology, it is important to know how mechanical properties vary with respect to changes in time, space and various chemical processes. This can be analyzed by extracting E from the force deflection data measured from SPMs at many points on the material (or cell) surface. Standard formulations developed for contact mechanics of

deformable substrates using rigid indenters [17, 51] are used to extract the E.

The viscoelastic characteristics of human platelets were measured using this technique [8] with E in the range of 1-50 kPa. The loss modulus which related to the viscous response was two orders of magnitude lower than the storage modulus. The cell relaxed during the load application and recovered fully when this external loading was removed, showing the recovery behavior of cells. The biomechanical changes exhibited by synaptic vesicles were studied in detail using force maps. The modulus values varied from 0.2 MPa to 1.3 MPa when these structures were exposed to various chemical environments. [34]. Hofmann et al. showed that the elastic moduli of the lamellipodial region varied from 10 kPa to 200 kPa in living chicken cardiocytes [33]. Force maps were used to measure the local mechanical properties of cytoskeletal elements. The stress fibers were 3 to 10 times as stiff as the surrounding cytoskeleton. The limitations of Hertz model in evaluating the force maps were also identified in this study [33]. The extending and retracting dynamics of protruding and stable edges of motile 3T3 fibroblasts showed that for the stable cell edges E was approximately 12 kPa. The leading edge had much lower modulus values equivalent to 3-5 kPa [7]. This study showed the limitations of using Hertz model to predict E, especially when the thickness of the sample allowed substrate effects to dominate. These limitations were also addressed in several other studies [8, 33].

The effect of various drugs on different cytoskeletal components of fibroblasts were investigated using the elasticity maps [39]. The elasticity maps showed that the actin filaments, which are the principal cytoskeletal component responsible for maintaining cellular tension, disassociated and correlated with decreased cellular rigidity when treated with certain drugs. These maps were used to study the modulus variations amongst different clusters of cell surface macromolecules such as receptors and ion channels [5]. The elasticity maps showed significant changes in local elasticity with regions underlying the receptor clusters appearing less stiff. The modulus of outer cell regions ranged from 50 to 120 kPa and around the nucleus ranged from 3 to 6 kPa. The E of human rhabdomyosarcoma transfectant cell line and NIH-3T3 mouse fibroblasts showed sharp increases for even mild chemical fixation [19]. This study

showed how mechanical properties of cells changed during chemical fixation using the modulus maps.

The above studies have shown that the modulus mapping technique is a very good tool for understanding the variations in E during cell migration, changing mechano-chemical environments and during cell fixation. This thesis implements this technique of force volume mapping. The indention technique used to understand the stress fields on thin polymer films in section 2.1 finds direct applications towards the way these force-deflection curves are used for predicting the modulus values, as discussed in section 3.3 of chapter 3.

Chapter 3

Modeling methods and geometry used for characterization of nano-scale films

This chapter discusses the modeling methods used in this study. Axisymmetric two dimensional and three dimensional meshes are generated to evaluate the stress fields evolving as a result of application of various boundary conditions such as for nano-indentation, tractive forces generated by cells etc. Also discussed in this section is the approach used for modeling the modulus maps that are generated using SPMs force-deflection data. The computational meshes are generated using meshing software TRUEGRID from XYZ scientific applications [48] while the analysis is performed via the general purpose finite element software ABAQUS [43].

3.1 Characterization of nano-scale films during nano-indentation

This section describes the modeling method used for analyzing the geometric effects of thin films during indentation and also the effect of varying the angle of indentation during these nanoscale indentations.

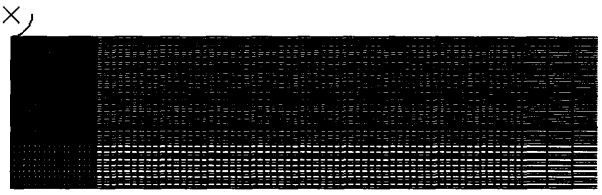

Figure 3-1: Finite element model used in simulations of polymer film indentation.

3.1.1 Modeling of indenter-substrate contact for analyzing the substrate effects

Figure 3-1 shows the finite element model mesh and boundary conditions for the simulations reported herein. This model included 34,476 nodes and 34,104 four-noded axisymmetric elements.

Both the material films and the spherical indenter exhibit axial symmetry, and are thus considered in a two-dimensional simulation. The indenter was modeled as an infinitely rigid material of radius $R = 25$ nm, which is consistent with the nominal apex radius of Si_3N_4 pyramidal cantilevers used in SPM-enabled nanoindentation [40], while the material films are modeled using linear elastic and, separately, hyperelastic constitutive relations for film thicknesses of 50, 175, 300, 600, and 1000 nm. The distal conical portion of the cantilevered indenter is not modeled in these simulations, as the typical maximum indentation depth implemented in related experiments [40] and in these simulations is less than R [40]. The contact between the indenter and the material film is assumed to be frictionless, and the nodes at the film/substrate interfaces are modeled as rigidly fixed, based on the assumption that the polymeric film is rigidly bonded to an infinitely rigid (or comparably so) substrate. A displacement controlled analysis is implemented to simulate the nanoindentation, and the output extracted from the simulations is that of the loading force P corresponding to the indentation depth h at each timepoint; quasistatic loading is thus assumed. The maximum indentation depth h_{max} for all simulations is 20 nm, except for the model for $t = 50$ nm where $h_{max} = 17.5$ nm was the maximum depth at which the FEA stiffness matrix converged for the given mesh density, element type/shape function,and

constitutive relation employed.

The Hertzian elastic contact model is the most widely used closed-form solution to calculate E of any material under generalized contact conditions. For small indentations ($h_{max} \ll R$), the paraboloidal indenter is well approximated as a sphere for which the Hertzian elastic solution exists. The relation between the depth of a spherical indenter and the corresponding applied load was formalized by Sneddon [42] based on the Hertzian formulation:

$$P_{sphere} = \frac{4}{3}\frac{E}{1-\nu^2}\sqrt{Rh^3}. \tag{3.1}$$

where ν is the Poisson's ratio of the sample (equal to 0.5 for ideally incompressible materials,and assumed to be 0.49 for mathematical tractability in the simulations herein). Thus E can be calculated directly from the output P-h response and chosen simulated R for a given material constitutive relation via equation 3.1, although it is important to note that equation 3.1 tacitly assumes linear elastic behavior of a semi-infinite, indented material. The nominal flow strain level ϵ applied to the material has been approximated in several forms, including: h/t, h/R and, most accurately, as

$$\epsilon = 0.2a/R. \tag{3.2}$$

where a is the radius of contact at the material surface [45]. The fraction of indentation depth h to film thickness t sampled is not an actual strain and is termed hereafter as f, where the diameter of the elastically deformed contact zone and thus likelihood from artifactual stiffening in P-h response due to the underlying substrate increases with increasing f.

The polymeric films considered herein are modeled as both linear elastic and, separately, hyperelastic materials. For the linear elastic case, three values of E were considered: $E_1 = 100\ MPa$,$E_2 = 10\ MPa$ and $E_3 = 0.5\ MPa$. These values are based on the experimental results from Thompson et al., obtained via SPM-enabled nanoindentation (Si_3N_4 cantilever of $R = 25$ nm) for thin film polyelectrolyte multilayers [40]. For the hyperelastic case, the strain energy function W for incompressible

materials was postulated by Mooney [31] and is given by

$$W = C_1(I_1 - 3) + C_2(I_2 - 3). \tag{3.3}$$

where C_1 and C_2 are the elastic constants and I_1 and I_2 are the first and second invariants of the Cauchy-Green deformation tensor [2].

Based on the above formulation, for an incompressible material with infinitesimal indentation depth h the Young's elastic modulus E can be expressed as

$$E = 6(C_1 + C_2). \tag{3.4}$$

Previous studies have shown that the widely applied infinitesimal strain models for nanoindentation yielded substantial errors in the estimated properties such as E for non-linear elastic materials [10]. The values for the elastic constants used in this hyperelastic analysis are $C_1 = 0.0235\ MPa$ and $C_2 = 0.060\ MPa$. These material constants are not chosen to represent a particular polymer, but rather to assess how the film thickness t and E independently affect the SPM-enabled nanoindentation response for a constitutive model that is more representative of polymeric materials than linear elastic models. The resulting value from equation 3.4 is $E = 0.50\ MPa$, which is consistent with one of the three linear elastic cases considered despite the clear difference in the constitutive relations.

For a given film thickness t, there exists a critical depth of indentation h_{cr} that depends on the mechanical properties of both the film and substrate, beyond which the force P required to attain a depth h increases due to the proximity of the film / substrate interface. This violates the semi-infinite film thickness ($t \gg h_{max}, R$) assumed by the Hertzian model, but h_{cr} is not easily identified a priori [32, 26]. A semi-analytical correction for this artifactual increase in stiffness due to finite film thickness proposed by Dimitriadis et al. [6] as:

$$P = \frac{16}{9} E \sqrt{R\delta^3}[1 + 1.133\chi + 1.283\chi^2 + 0.769\chi^3 + 0.0975\chi^4] \tag{3.5}$$

where

$$\chi = \sqrt{\frac{R\delta}{h}} \tag{3.6}$$

is the correction factor due to finite thickness.The maximum film thickness for which this correction is applicable is stated by Dimitriadis et al. as $h < 12.8R$ [6]. This restriction is based upon the assumption that the material behaves in a linear elastic manner for maximum strains less than or equal to 10%,which may or may not be true for a given material. Hence, in this study the thickness correction would apply for film thickness $t < 320\,nm$. Equation 3.5 can then be used to calculate E for films of ostensibly identical or systematically varied mechanical properties, of varying thickness. Mahaffy et al. [21] have shown that the value of the Poissons ratio also affects the calculation of E when indenting samples of finite thickness. Experimental results [21] have shown that as the Poissons ratio increases from 0.3 to 0.5, the depth h_{cr} at which the underlying stiff substrate artifactually stiffens the measured response actually decreases. This means that due to the high Poisson's ratio of polymers, even in μm-scale thick areas of experimental samples such as living cells, the Hertz model will fail to predict accurately the elastic properties.

3.1.2 Modeling of indenter-substrate geometry to consider effects of varying SPM indenter angle on measured mechanical properties

This section deal with the modeling of inclined contact geometry for analysing the effects of angle of indentation on the mechanical properties of the materials. The indenter is modeled as a rigid material while the sample substrate is modeled as a deformable material. The substrate is assumed to be incompressible. The model is assumed to be linear elastic and isotropic. The angles of indentation θ used are $0°, 6°, 9°$ and $15°$. For $\theta = 0°$ angle of indentation only one quarter of the full model is used due to the four-fold symmetry of boundary and loading conditions. Figure 3-2 shows the indenter and sample geometry at $\theta = 0°$. For all the other cases where angle of indentation is different from $0°$, half of the full geometric model is used. The

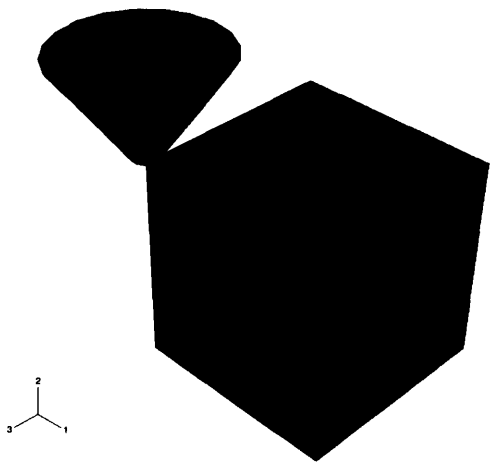

Figure 3-2: Model showing 0° angle of indentation.

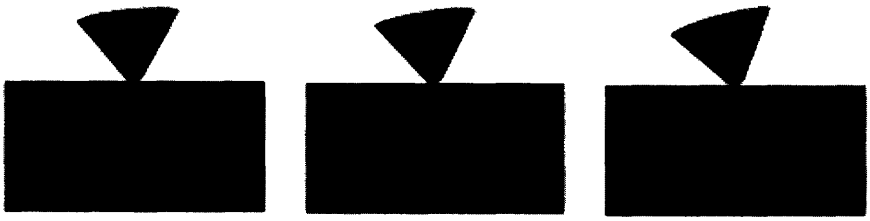

Figure 3-3: Bulk Model showing 6°, 9° and 15° angle of indentation.

reason for using the half-model is because both the boundary conditions and subsequently the stresses resulting from these boundary conditions are symmetric along only one plane. The planes of symmetry here are $x - y$ plane and $y - z$ plane. Figure 3-3 shows the indenter and sample geometry at $\theta = 6°, 9°$ and 15°. In order to understand the effect of thickness as the angle of indentation is changed, two cases are analyzed. One case is where the thickness of the sample is equivalent to 300 nm, which would be sufficient to model the material as bulk with the induced stresses confined entirely within the geometry. The boundary conditions used for modeling indentation are free slip between the indenter and the substrate during contact. For evaluating the effect of thickness, a thin film of 50 nm thickness is modeled, as shown in figure 3-4. For estimating E, the Hertzian formulation shown in Equation 3.1 is used. The methodology as followed in section 3.1.1 for the axisymmetric case is used

Figure 3-4: Model of 50 nm thickness showing 6°, 9° and 15° angle of indentation.

here.

The two dimensional concept is extended to the three dimensional (3D) analysis. Eight noded brick elements are used to model the geometry. In 3D, 24,471 nodes and 21,978 elements are used for modeling the bulk and 50nm thick samples during the 0° angle of inclination θ. Here, 41,860 nodes and 38,016 elements are used to model the bulk sample for 6°, 9° and 15° angles of indentations while 48,300 nodes and 43,956 elements are used to model the 50 nm-thick sample for θ= 6°, 9° and 15° indentations.

3.2 Modeling of substrate geometry to evaluate effects of focal adhesions on substrate deformation

A three-dimensional finite element mesh made of brick elements is modeled to study the effects of forces exerted by focal adhesions on substrates. It is assumed that the cell is semicircular with a radius of 7.5 μm when resting on a substrate. The cells adhere to the substrate through focal adhesions and the total area of the focal adhesion is assumed to be 1 μm^2 [1]. Because of the assumption that the cell-substrate geometry is circular in shape, only one quarter of the geometry is modeled. The model is shown in figure 3-5. The material model is assumed to be linear elastic, isotropic and incompressible. The total area in all the focal adhesions is conserved. This means that if there are 4 focal adhesions and the total modeled focal contact area is equivalent to 1 μm^2, then the total modeled contact area for 8 focal adhesions is also equal to 1 μm^2.

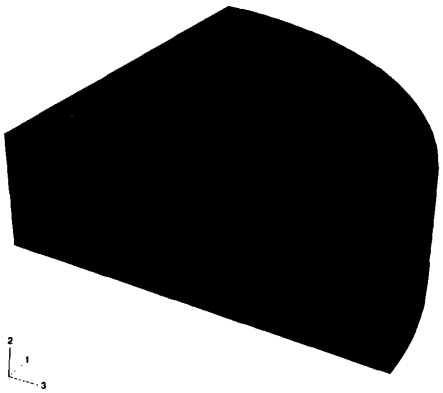

Figure 3-5: Finite element model of substrate used for simulation of cell-substrate interactions.

Displacement boundary conditions are prescribed to all the points on the focal contact points. These prescribed boundary conditions are given in such a way that the traction evolving from these would equal to experimental conditions [1] of $\sigma_t = 5$ nN/μm^2. The total number of nodes used here is 16,464 and the number of elements is 14,355 for modeling 4 focal adhesions per cell; while 28,668 nodes and 25,344 elements are used for modeling 8 focal adhesions per cell. The modulus of films used in this study are E= 18 kPa, 180 kPa and 1800 kPa and the thickness of the films t are 6 μm, 3 μm and 0.5 μm.

3.3 Modeling of modulus maps

Elastic modulus values of each point on the cell surface are calculated by evaluated the force deflection curves derived from force volume mapping. The cells used are human umblical vascular endothelial cells (HUVECs). In force-volume mode, the SPM cantilever is scanned across the sample [51] and the force spectrum recorded at each step. Force maps of 32 x 32 points are created across a 85 μm by 85 μm cell-substrate area. Figure 3-6 shows the image of the cell, for which modulus at each point in the cell is evaluated. Each point shown in figure 3-6 is a force map, which

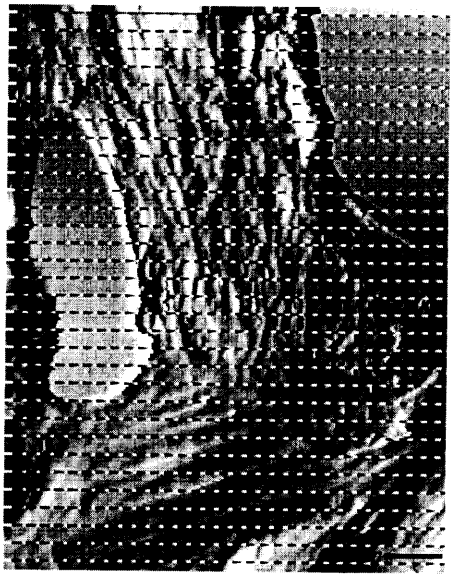

Figure 3-6: Image of the HUVEC cell.

consists of 32 x 32 force curves. The scanning speed is 1.49 lines/sec which gives the total time for measuring as 25 minutes. This time period is very large when living cell imaging is done. Many cell types will change intrinsic mechanical characteristics over this time period [51]. However, this factor is not considered here as this study attempts only to implement modulus mapping as a general technique. The stiffness of the cantilever k is 0.06 N/m,and the half angle of the conical tip is 38°.

To extract E from the force curves, Sneddon's and Hertzian model for elastic indentation on a flat, soft sample by conical geometry is used [17, 42]. Based on the cantilever deflection, and the formulations for contact mechanics developed by Sneddon, the equation for conical tip can be expressed as follows,

$$h = \sqrt{\frac{\pi}{2}\frac{1-\nu^2}{E}\frac{F}{tan\alpha}} \tag{3.7}$$

On soft samples, the cantilever deflection $d(z)$ is a function of piezo movement z and indentation depth h given by

$$d(z) = z - h. \tag{3.8}$$

The force exerted by the cantilever P is given by

$$P = kh. \tag{3.9}$$

where k is the stiffness of the cantilever [51].

Combining equations 3.7,3.8,3.9 the final form used is

$$d - d_0 = z - z_0 - \sqrt{4s}\sqrt{d - d_0}. \tag{3.10}$$

where z_0 is the contact point at which the sample starts showing deflection and d_0 is the free cantilever deflection [19]. The value s is given by

$$s = \frac{\pi}{8}\frac{1-\nu^2}{E}\frac{k}{tan\alpha}. \tag{3.11}$$

From equation 3.10 ,E is evaluated from each force curve through a non-linear fit [23]. Hence, by extracting E at each point, a complete modulus plot of the cell surface can be obtained.

Chapter 4

Results and Discussion

4.1 Characterization of mechanical properties of thin films

4.1.1 Effects of film thickness on estimated E

Results

The variation of load P with depth h on a log_{10} scale is shown in figure 4-1a, for film thickness $t = 1000$ nm and $E = 0.5$ MPa. The slope of 3/2 is consistent with equation 3.1, which is the Hertzian formulation.

The value of E calculated is within 10% of the input value of E, which confirms the well known result that for a linear elastic material of given E and film thickness t, the contact response can be approximated by the Hertzian model. The von Mises stress distributions shown in figure 4-1 b are well confined within the film.

The distributions of von Mises stress contours for a linear elastic case of $E = 10$ MPa and a range of film thickness $t = 50$, 600 and 1000 nm are shown in figure 4-2. These simulations show how stress fields are transferred through the thin films, for a given value of E. The stresses are confined to approximately to 10% of t. This shows that for a given critical thickness, E can be predicted to within 15% of the actual value, using the Hertzian formulation given by equation 3.1. The fundamental

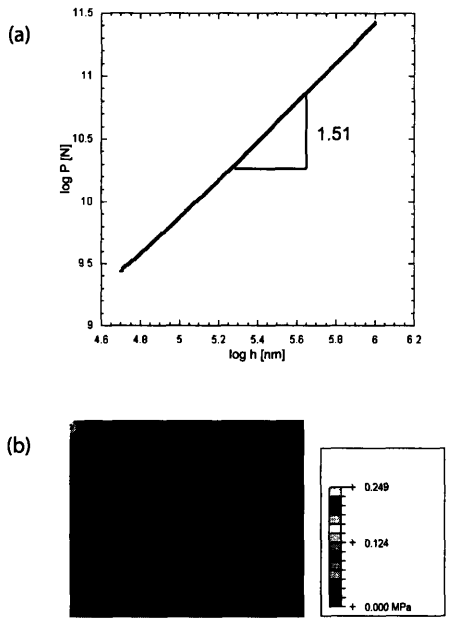

Figure 4-1: Finite element response of elastic film when $t = 1000$ nm and $E = 0.5$ MPa: (a) verification of Hertz model given in equation 3.1 and (b) von Mises stress.

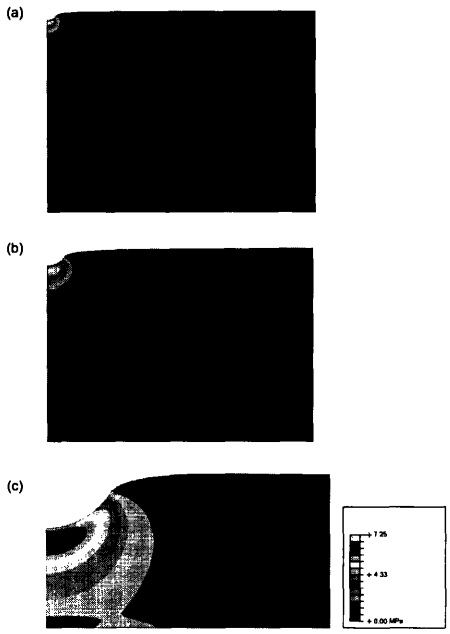

Figure 4-2: Von Mises stress distributions for films of varying thickness t and $E = 10$ MPa: (a) $t = 1000$ nm, $h = 20$ nm; (b) $t = 600$ nm, $h = 20$ nm; (c) $t = 50$ nm, $h = 17.5$ nm.

assumption while calculating E is that the material is linear elsatic. When the thickness is below the critical value, the underlying rigid substrate begins to influence the prediction of E which is shown in figure 4-3. E calculated from the P - h response using equation 3.1 is shown in figure 4-3 as a function of t. When the film thickness is on the order of maximum depth of indentation h_{max}, this results in a significant increase in calculated E with respect to the actual E that is dictated by the constitutive equation. Figure b shows the trend to be similar for all values of E (due to the linear elastic assumption). Figure 4-3c shows the value of power law of equation 3.1 for a film that is of $t = 50$ nm and $E = 100$ MPa. The value of 1.67 deviates from the theoretical value of 3/2, demonstrating the lack of applicability of the model. The model which was originally intended for macro-scale contact mechanics, or for linear elastic case with semi-infinite material dimensions, does not apply here due to the film finite thickness.

Many polymeric materials are highly nonlinear in their behavior within the elastic regime. In order to understand the non-linear material behavior, the Mooney-Rivlin model has been applied. This shows that the overestimation of E is very similar in behavior to the linear elastic case. These data demonstrate that the finite thickness effects are seen in estimations of E, even when modeled using constitutive material models which are more representative of polymers. Figure 4-4 that the calculated E is close to the bulk or input value for $t > t_{cr} = 200$ nm and maximum indentation of $h_{max} = 20$ nm ($\epsilon_{max} = 40\%$). Figure 4-4 shows the calculated E to be close to the bulk value for a $t > t_{cr} = 200$ nm with a maximum indentation depth of 20 nm. The value E is overpredicted for both constitutive models, the linear elastic and hyperelastic cases. The t_{cr} at which E is overpredicted increases for hyperelastic model. That is, the nonlinear elastic deformation of the material relaxes the film thickness constraint.

Figure 4-5 shows the variation of E with respect to the dimensionless parameter $f = h_{max}/t$. For samples that are of nanoscale thickness (eg. t=50 nm) or when maximum indentation depth $h_{max} > 0.1t$, the calculated E increases by more than a factor of two for larger indenter radius R. Here, $R = 2500$ nm and 25 nm, for the same

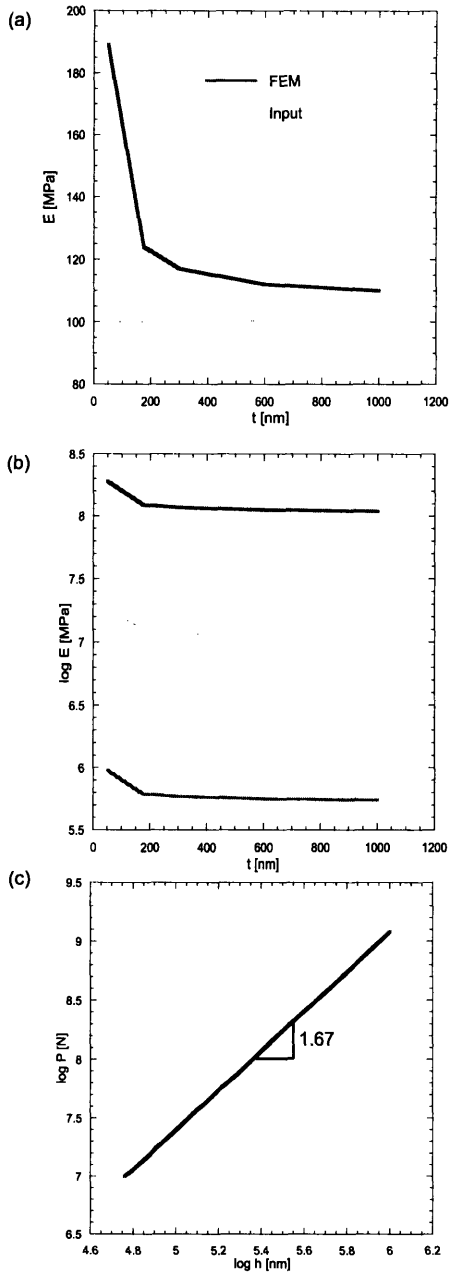

Figure 4-3: Comparison of experimental and calculated E for linear elastic films as a function of film thickness t and constant indentation depth $h = 20$ nm: (a) $E = 100$ MPa; (b) $E = 100$, 10 and 0.5 MPa; (c) Deviation from the Hertzian prediction of 3/2 power law for $t = 50$ nm and $E = 100$ MPa.

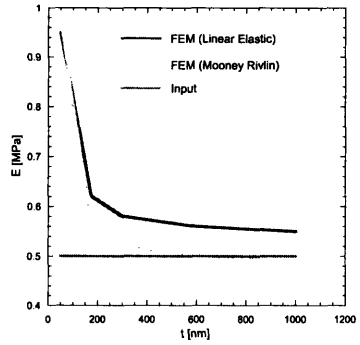

Figure 4-4: Comparison of E calculated using equation 3.1, assuming either a linear elastic or a hyperelastic constitutive model (Mooney Rivlin, equation 3.3) for E = 0.5 MPa.

value of f. Naturally, strains induced by the larger indenter radius are much lower compared to smaller indenter radii [6]. However, the calculated E are very high for larger radii (figure 4-5b). The differences in calculated E values when a 50 nm thick sample is indented to h_{max} = 12.5 nm indenter radii R of 25 nm and 2500 nm are shown in figure 4-5b. Figure 4-6a shows the difference in estimated E when compared to the actual value of E = 10 MPa. Figure 4-6b shows the $P - h$ response for the bulk and t = 50 nm samples when these are indented to h = 12.5 nm. Overprediction of E occurs due to the substrate proximity effects which are shown in figure 4-6b-d. When compared to the smaller indenter radii, the larger radii induce lower stresses when indented to same depth. However, the transmission of stresses from the larger indenter radii to the substrate is different because of the correspondingly larger contact zone of elastic deformation. This critical factor brings out a unique correlation between the indenter geometry and shape of the stress contours for a given substrate thickness. The stress distributions become flatter as the indenter geometry becomes larger, spreading in the lateral direction compared to the loading axis as is evident from figure 4-6d. One more factor that contributes to the overprediction of E is the fact that the nanoscale films are very strongly adhered to the support structure. Due

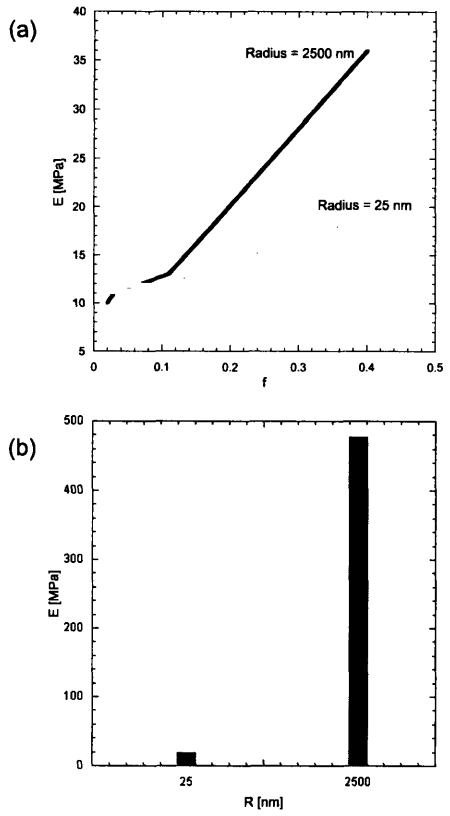

Figure 4-5: Effect of indenter radius R on calculated $E = 10$ MPa: (a) as a function of fraction of film thickness sampled $f = h_{max}/t$; (b) for a linear elastic film of $t = 50$ nm indented to a depth of $h = 12.5$ nm with indenters of nanoscale and microscale radii.

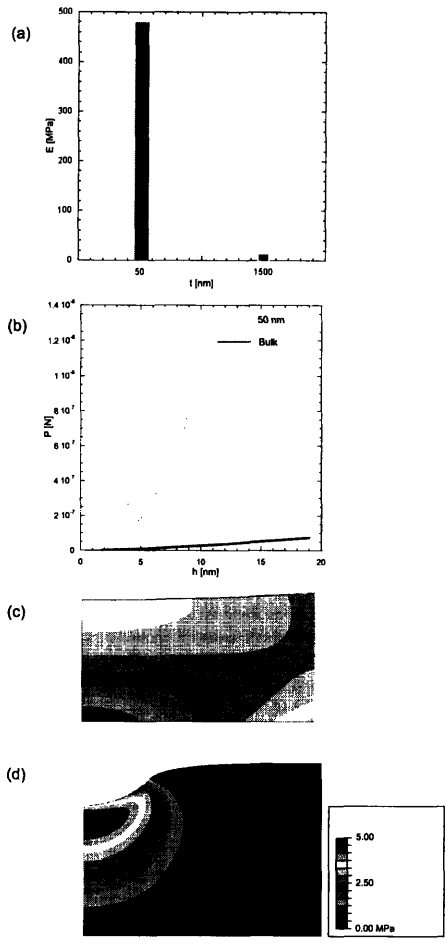

Figure 4-6: Demonstration of substrate proximity effects on overestimation of thin film E, accentuated by the use of large indenter radii: (a) Calculated E for an input modulus of 10 MPa and indentation depth of 12.5 nm; (b) Corresponding load-depth (P - h) response compared to that of a bulk sample of same input modulus; von Mises stress distribution for film thickness $t = 50$ nm and $h = 12.5$ nm for (c) $R = 2500$ nm; and (d) $R = 25$ nm.

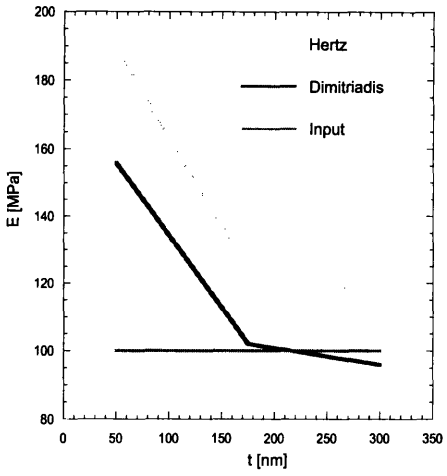

Figure 4-7: Comparison of Hertzian and Dimitriadis [6] models of elastic modulus calculation for input $E = 100$ MPa. Identical trends were observed for $E = 10$ MPa and 0.5 MPa.

to the smaller thickness along the loading axis, the material more strongly resists lateral deformations during the indentation process, inducing larger stresses. This becomes a critical factor when the indenter radius becomes large enough to increase the contact stress zone both laterally and vertically.

Models proposed by Dimitriadis et al. [6] directly consider the effects of finite thickness of mechanical properties estimated from the the P - h response. Figure 4-7 shows how the classical Hertzian model formulated using equation 3.1 compares with the semi-analytical model for a linear elastic material which shows the variation of E with t. This model is superior to the Hertzian model in estimating the E. However even this model overpredicts E below a certain value of film thickness. This comparison between these analytical models is important for two reasons. First, a model which was originally developed for macroscopic contact can be extended to linear elastic samples of finite thickness if a finite thickness correction factor is used [6]. Secondly, as shown in figure 4-7, even with thickness-corrected Hertzian formulations, overestimation of E as the thickness of t is reduced to the nanoscale. Table 4.1.1 shows the effect of dimensionless parameter f on the amount of error in calculated E when the film thickness is reduced or the depth of indentation is reduced, for

two indenter radii.

Effect of increase in f on contact strain % and predicted E expressed as a function of indenter radius R.

t[nm]	f	R[nm]	ϵ	E_{input}[MPa]	Overestimation of E [%]
18000	0.03	2500	11.69	10	6
9000	0.07	2500	13.49	10	16
5250	0.11	2500	13.98	10	32
1500	0.40	2500	38.86	10	255
1000	0.02	25	28	10	10
600	0.03	25	28.29	10	12
300	0.07	25	28.26	10	16
175	0.11	25	30.25	10	24
50	0.35	25	43	10	89

It is seen that both ϵ as well as simulated E increase as f increases. As the value of f becomes greater than 0.1, the error increases significantly, with % error in E of approximately 255% for $f = 0.4$ for $R = 2500$ nm, and 89% for $f = 0.35$ when $R = 25$ nm. The reason for this significant increase in error, especially for $R = 2500$ nm, is because of the manner in which the stress fields redistributes around the indentation zone as shown in figure 4-6c. The results discussed above are derived based on several simplifying assumptions, including axisymmetric (rather than fully three dimensional) geometry, and neglect of viscoelastic material models.

Discussion

The technological and processing advancements in materials processing of films have enabled fabrication of films that are on the order of 100 nm or less in thickness. This makes possible a wide range of applications such as synthetic substrata for understanding cellular functions [37]. This thesis addresses the applicability of Hertzian analysis in estimation of E for polymeric thin films, when these films are deformed through multi-axial loading conditions.

Figure 4-2 a-c shows that below a critical thickness t_{cr} and for a given depth of

indentation h_{max}, the Hertzian model is valid, provided linear elasticity is an accurate material model. This means that the accurate estimation of E is possible, provided that the depth of indentation is below h_{cr} for a given film thickness. The measured value of E is accurate for indentation depth less than 20 nm which is the critical thickness (for radius of indenter = 25 nm and E greater than 0.5 MPa) , beyond this thickness the measured value of E is within 15% of the actual bulk value. The reasons for this overestimation of E for larger indentation depths are enumerated below.

As shown in figure 4-3c the power law exponent derived from the Hertzian formulation starts to increase as the film thickness decreases from 1000 nm to 50 nm. This deviation of h_{max} greater than 10% of film thickness actually increases the calculated E values due to the proximity of substrate. This inaccuracy of E becomes a critical issue when the substrate compliance contributes significantly to cellular morphology and physiology [40, 35]. The trend of overestimated E is seen even for the case of a hyperelastic material model, which ideally would resemble the polymer deformation more closely than linear elastic model. As seen from figure 4-4, for $E = 0.5$ MPa. In a hyper elastic material, t_{cr} is reduced from 300 nm to 200 nm. This shows that E can be extracted accurately for a larger value of f, without substrate artifacts, when this model is used.

Figure 4-6c-d shows that the overestimation of E occurs even with larger indenter radius. Larger radii induce smaller strains, but the stress field distributions are much different for larger R as the film thickness decreases the transfer of stresses to the substrate also increases. This demonstrates that even though the larger radius of indenters induces lower contact strains, this does not necessarily imply a more accurate estimation of E. The overestimation of E with increasing R is shown in figure 4-5 a-b.

For accurate measurement of mechanical properties, it is ideal if the indenter radius is large enough to maintain mechanical strains below the elastic limit. This is not often the case, as most cantilever probe radii are of the order of 25 nm. Such small R induce strains that are greater than 10% for indentation depths that are less than 20 nm. For such indenter geometries, the Hertzian model applies for $t > 300$ nm, as shown in figure 4-3a. Even for contact strains in excess of an estimated elastic

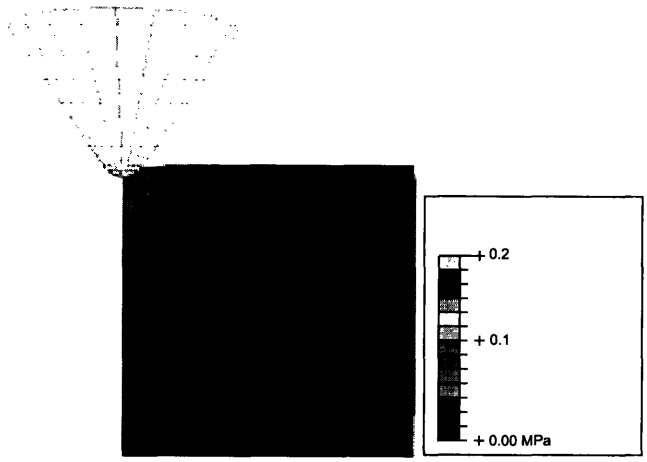

Figure 4-8: von Mises stress distribution in bulk film for $\theta = 0°$ and $h = 13$ nm.

limit, the overestimation of E does not exceed 89%, as shown in Table 4.1.1. This indicates that changes greater than this could be due to real microstructural changes or external artifacts other than film thickness t.

4.1.2 Effect of indenter angle on estimated E

Results

While section 4.1.1 focused on understanding the effect of thickness on estimations of modulus, this section will enumerate the results from the analysis for indentation at inclination angles $\theta = 0°, 6°, 9°$ and $15°$. The maximum indentation depth h_{max} in all cases is 13 nm. The indenter and sample geometry for bulk and thin film cases of various inclination angles are shown in figure 3-2, figure 3-3 and figure 3-4. As shown in figure 2-3, as the angle of indentation increases the contact area between the indenter geometry and film also increases. This increase in contact area subsequently affects the accuracy of calculated mechanical properties [25]. This section decouples the effect of angle of indentation during nanoindentation from finite film thickness. Figure 4-8 shows the von Mises stress distribution for $\theta = 0°$ for a thick(μm-scale) film. This shows that the stresses are confined inside the film. Figure 4-9 shows the von Mises stress distributions for $\theta = 0°$ for a film of $t = 50$ nm. This figure clearly

Figure 4-9: Von Mises stress distribution for $\theta = 0°$ angle of indentation and $h = 13$ nm and $t = 50$ nm thick film.

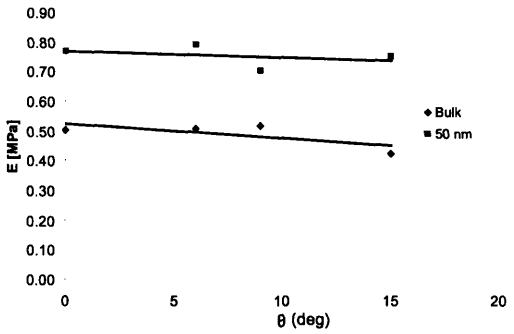

Figure 4-10: Effect of probe inclination angle θ on estimation of E values.

shows the stresses to be no longer confined inside the film. The modulus value E does not change with θ as shown in figure 4-10. All the calculations for E are based on the assumption that the indenter geometry is spherical. During experiments, this assumption does not hold true as seen in figure 4-10. This clearly demonstrates the deviation from spherical geometry during indentation at larger θ. The invariance of calculated E as a function of θ holds true for both the bulk geometry and for the thin film case where $t = 50$ nm. As seen from figure 4-10 for the bulk case, the calculated value does not change from the input or actual E value by more than 10%.

However, for the thin film case ($t = 50$ nm), there is an increase in estimation of E

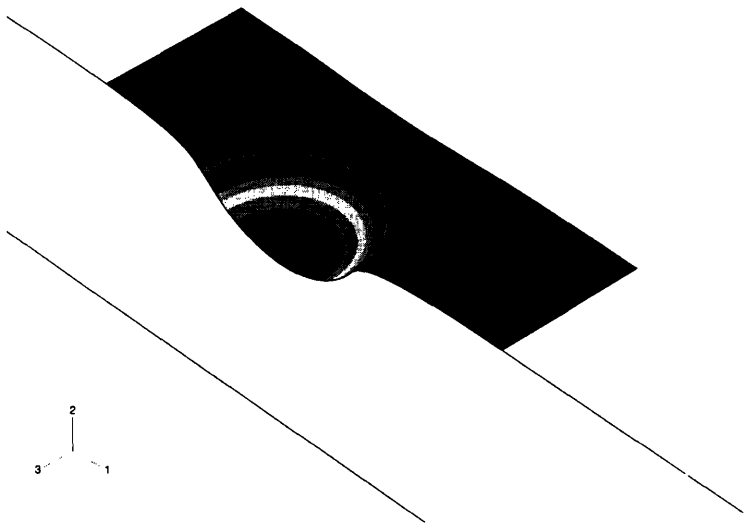

Figure 4-11: Contact pressure distribution on a film of $t = 50$ nm and $\theta = 15°$.

as shown in figure 3-3. This increase in E when compared to the bulk value is because of the decrease in film thickness and relative increase in substrate proximity, leading to overestimation of E. However the value of E does not change with θ even for the thin film case, which demonstrates that θ does not greatly affect the estimation of E and it is only the change in film thickness that strongly affects the calculated E.

Figure 4-11 shows the von Mises stress distribution for the case of $t = 50$ nm and $\theta = 15°$. As shown in Figure 4-12, the value of peak contact pressure p_{max} remains the same for a given film thickness. The force range during typical scanning process using SPM is of the order of 1 nN. This force range has been found to induce destructive effects and changes in cellular morphology eventually leading to cell death [8, 53]. The contact pressure distribution shown in figure 4-12 corresponds to an average force of 100 pN for $h_{max} = 13$ nm.Here, p_{max} does not change with the θ, but does increase with decreasing t. It is seen from figure 4-12 that for a given t, p_{max} is constant with θ.

One of the critical parameters of interest is the manner in which shear strains change as a result of changes in θ and t. The behavior of changes in these strain fields

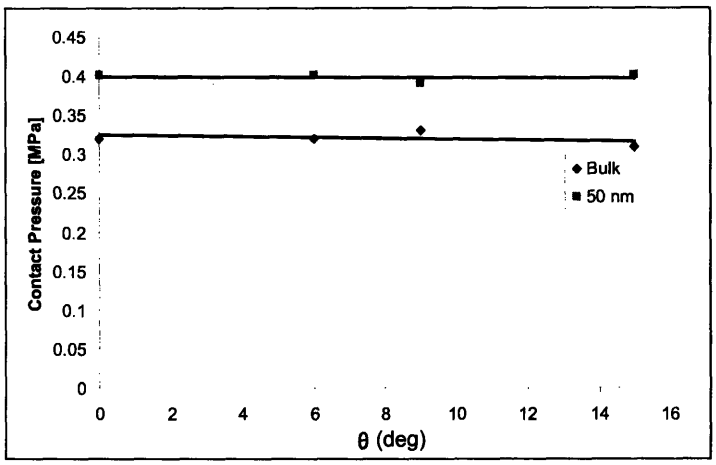

Figure 4-12: Contact pressure distribution as a function of t for different θ.

are important because of several reasons. First the distribution of these surface strains would help to understand how indentation affects the regions near the indentation area which would subsequently help in designing polymeric films that can limit or increase the strain fields due to applied loads. Secondly, the range of E analyzed in this thesis is similar to that of substrates that serve as extracellular matrices for cells. Hence, thickness-dependent changes in strain field distributions of these thin films may help to better understand how strain is transmitted under cellular traction.

Figure 4-13 shows the shear strain distributions (ϵ_{12}) for the case of a thin film. The strain field extends down to the bottom of the film with both positive and negative shear strains acting through the film. This figure also shows that during nanoindenation, the multiaxial loading state causes the the maximum shear strain to exist not on the surface but within the film. Figure 4-14 shows the magnitude of ϵ_{12} for $\theta = 6°$, expressed as function of film thickness along the indenter profile in direction normal to the film surface. The figure shows that the magnitude of shear strain increases as thickness t decreases. The width over which shear strain is non zero, is defined as distance S in figure 4-13. S is $\approx$ 50 nm for the bulk film case. As the film thickness decreases, S increases to 80 nm. This shows that both the magnitude and extent to which shear strain extends increase with decreasing t. Figure 4-15 shows the magnitude and spread of shear strains S as a function of θ.

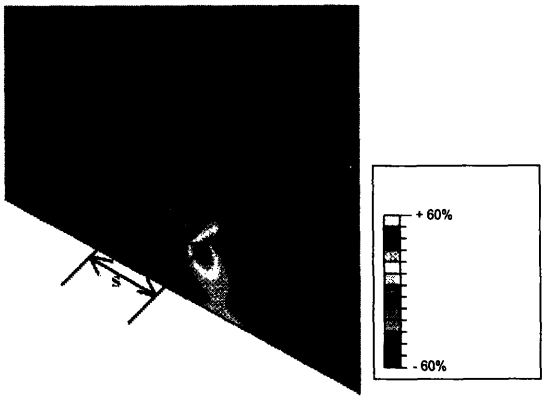

Figure 4-13: Shear strain distribution on a film of $t = 50$ nm and $\theta = 15°$ for $E = 0.5$ MPa.

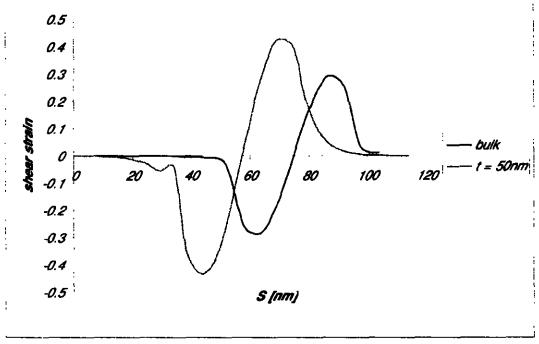

Figure 4-14: Shear strain distribution expressed as a function of S, on a bulk and thin film for 6° angle of indentation .

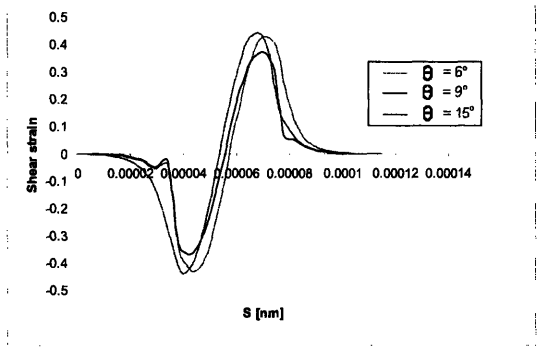

Figure 4-15: Shear strain distribution expressed as function of S for $t = 50$ nm and $\theta = 6°, 9°$ and $15°$.

Figure 4-15 demonstrates that neither the magnitude nor distribution of ϵ_{12} change when θ is changed. This means that for a given t, the magnitude and distribution of ϵ_{12} are not affected strongly by θ.

Discussion

The parameters E, p_{max}, and ϵ_{12} show no significant change as a function of θ. There are several reasons for the this behavior, as discussed below.

Throughout this analysis, the maximum indentation depth was 13 nm, approximately equivalent to the indenter radius $R = 25$ nm. This means that even with the change in θ as high as 15°, the spherical geometry would dominate the stress field (and the conical part of the indenter would not contribute). Because of this equivalence, the contact geometry was invariant with θ in all cases analyzed.

In this analysis, the indentation load application is allowed to occur normal to the film whereas in experiments the load is applied at an inclined angle θ. This means that there would be two components of force, one along the long axis of the cantilever and one normal to the long axis of the cantilever. The component along the axis of the cantilever is responsible for the drag and external torque during nanoindentation [25].

The contact pressure distribution and maximum contact force exerted are critical parameters during nanoindentation. During the nanoindentation process, for cells to

exhibit recoverable deformation behavior it is essential to keep the indentation forces below 1 nN [53]. It is seen here that the forces are below this level during the nanoindenation process, hence demonstrating the fact that during nanoindentation, if the indentation depth is kept to a point where only a spherical geometry dominates the indentation contact, cells could be indented non-destructively.

4.2 Effect of film stiffness and thickness due on focal adhesion induced stress and strain fields

Results

As described in Chapter 1, one direct application of these nanoscale polymeric films is in the field of bioengineering. These films are used as synthetic substrata to culture cells and subsequently understand cellular physiology as a result of variation in the mechanical properties of these substrates. These films will be under multiaxial loading conditions when adhered cells are fully confluent, due to the traction exerted by the cells. The aim of section 4.1.1 and 4.1.2 was to quantify the effect of film thickness and angle of indentation on calculated film properties. In this section, we attempt to characterize the deformation of these films, now cell substrates, as a function of focal adhesions as a function of film E.

The range of E and the type of boundary conditions used in this study are described in chapter 3. For this study the focal adhesion traction stresses were in the range of 3 nN/μm^2 - 5 nN/μm^2 [1]. Figure 4-16 shows the von Mises stress distributions for the case of $t = 0.5$ μm , when the prescribed displacements are applied to obtain the desired traction. The boundary conditions prescribed are on a film of elastic modulus $E = 18$ kPa. As seen from figure 4-16 the stresses exerted on these films are highly localized. This agree well with experimental studies that showed that the stresses exerted by cells onto the substrate through focal adhesions are highly localized and do not spread over a large area [1, 29]. One of the critical questions this

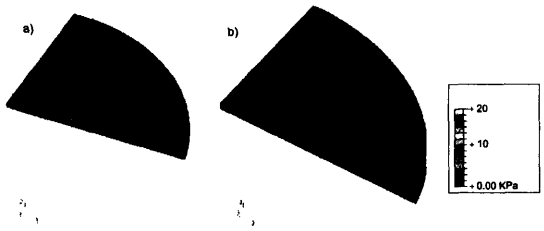

Figure 4-16: Von Mises stress distributions for (a) four and (b) eight focal adhesions per cell in a 0.5 μm thick film of $E = 18$ kPa.

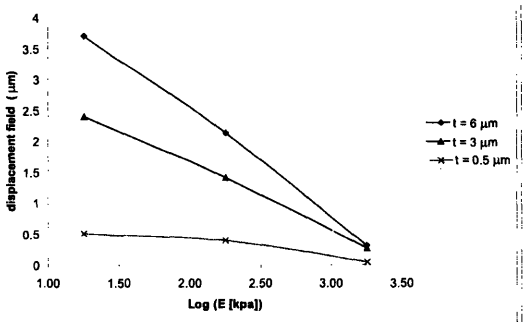

Figure 4-17: Distance to which the displacement field ($u = 1$ nm) is felt through the thickness of the geometry as a function of E, for 4 focal adhesions/cell.

thesis attempts to answer is how the thickness of the film influences the stress and strain fields within the film due to cellular focal adhesion-induced surface traction. Figure 4-17 and figure 4-18 show the displacement field through the film thickness, when similar tractions are exerted by 4 or by 8 focal adhesions per cell. These figures show that the extent to which the film displaces decreases as E increases, regardless of the number of FAs. The data collected through the thickness are at the points directly normal to the focal adhesion area, where the displacement field is maximum. Figure 4-17 and figure 4-18 suggest that the change in the extent to which the displacement field extends is not significantly different between 4 and 8 focal adhesions/cell, and the trend followed by both as a function of E are similar. However, for the case of films with thickness of $t = 0.5$ μm, the displacement field extends through the entire

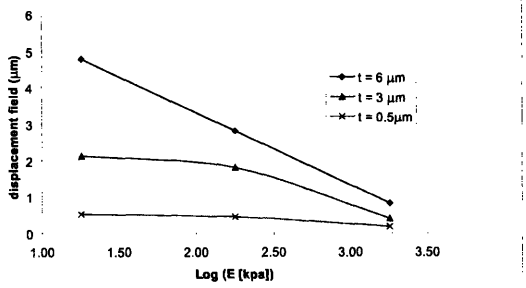

Figure 4-18: Distance to which the displacement field ($u = 1$ nm) is felt through the thickness of the film as a function of E, for 8 focal adhesions/cell.

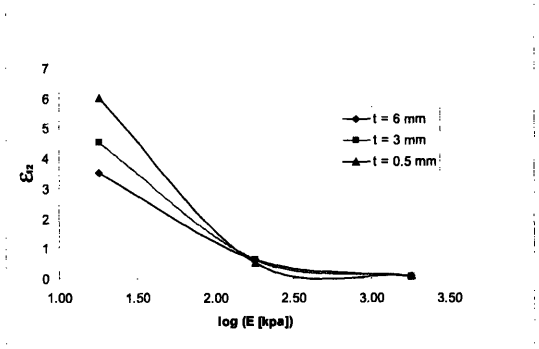

Figure 4-19: Magnitude of surface shear strain felt on top of the substrate as a function of modulus for 4 focal adhesions/cell.

film thickness. This means that there will be finite thickness effects for films of $E \leq$ 18 kPa for $t < 0.5$ μm.

One of the parameters of interest in tissue engineering is the magnitude and distribution of strains due to traction exerted by living cells against a given substrate. Figure 4-19 and figure 4-20 quantify the shear strain on the surface as a function of distance from focal adhesions. The trend of shear surface strains exerted by focal adhesions is the same for both the four and eight focal adhesions/cell, with the magnitude of shear strains decreasing as E increases. It is seen that in the case of 8 focal adhesions/cell, the strain magnitude is almost an order of magnitude greater than that for 4 focal adhesions/cell, even though the total applied traction in both these cases was similar.

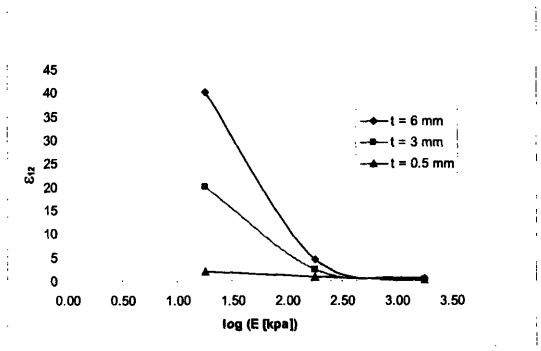

Figure 4-20: Magnitude of surface shear strain felt on top of the substrate as a function of modulus for 8 focal adhesions/cell.

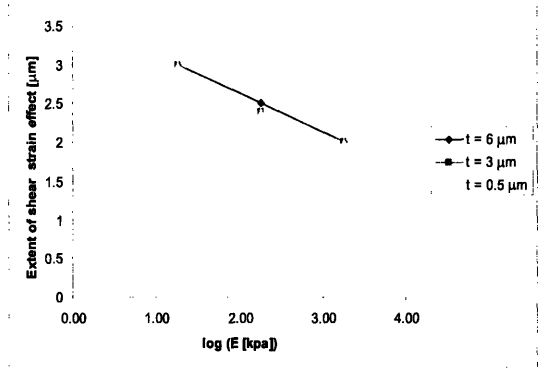

Figure 4-21: Extent to which shear strains are felt when traction are exerted by cells, for 4 focal adhesions/cell, expressed as a function of E.

The extent to which surface shear strains extend is quantified in figure 4-21 and figure 4-22. Both figures show similar trends, regardless of the number of FAs/cell. Also, the extent to which the shear strains extend in 4 FAs/cell are greater than 8 FAs/cell for a given E and t. This could indicate that the spread of the strain field would decrease as the number of focal adhesions increases, and the force is redistributed in the cell.

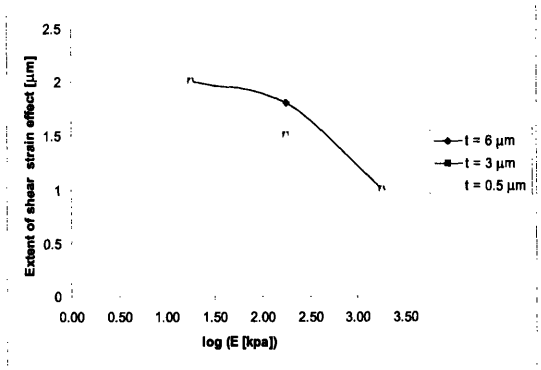

Figure 4-22: Extent to which shear strains are felt when traction is exerted by cells on the substrate, for 8 focal adhesions/cell expressed as a function of elastic modulus E.

Discussion

Figure 4-17 and figure 4-18 show the extent to which the displacement extends through the substrate. This means that as the number of focal adhesions increases (typically around 300 for fibroblasts [30]), the extent to which the focal adhesion-induced displacement is affected by the underlying film thickness varies. The combined effect of all these focal adhesions from a single cell onto the film remains to be analyzed.

The magnitude and extent of surface shear strains exerted are based on few focal adhesions in this study. In actuality there are millions of cells each having hundreds of focal adhesion points anchoring to the film. This may induce film deformation that might differ from what is proposed here. Even then, this study provides preliminary results on how film thickness and elastic stiffness affect transmission of forces due to cell adhesion. The FA area may also play a major role in exerted stresses and strains. This thesis develops all results based on a single combined area of 1 μm^2 exerting σ_t = 5 nN/μm^2. In actuality, this value differs from FA to FA and also varies among different cell types. The reason for decoupling E and t here to study cellular adhesion is because, in ideal experimental conditions, there are several variables that need to be considered which would make analysis extremely complex and time consuming such that it would be difficult to infer geometric and mechanical effects from a cell population study.

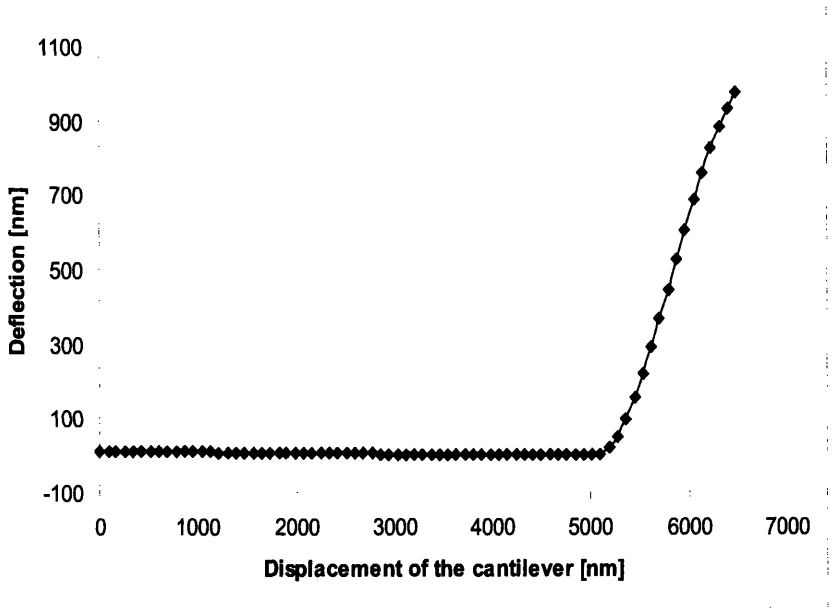

Figure 4-23: Displacement of cantilever vs deflection measured on the cell.

4.3 Modulus mapping of living cells

Force-volume mapping is one of several tools which can be used to characterize E of thin films and of cells. The topic of interest in previous sections was to extract and evaluate the mechanical properties of polymeric thin films, using formulations based on contact mechanics when these films were subjected to multiaxial loading conditions. This section deals with extracting E from the P - h responses obtained from force-volume experiments.

Figure 3-6 shows the region on a human umblical vascular endothelial cell (HUVEC), on which the P - h responses were obtained. Figure 4-23 shows the deflection versus displacement of cantilever for one point on the cell. Equation 3.10 (conical indenter, discussed in Chapter 3) is used to extract E at each such point on the cell. A small section of the cell shown in figure 4-24 is used for demonstrating the extraction of E. The curves as shown in figure 4-23 are normalized such that the height and deflection values start from 0. The slope of the curve changes as soon as the cantilevered probe comes in contact with the cell. This point at which the value of deflection starts

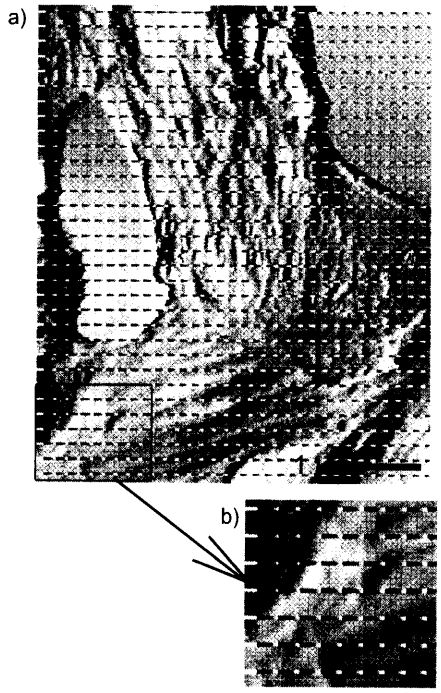

Figure 4-24: (a) Cell image showing the data points on which P - h curves were taken. (b) Image of smaller section of cell used for analysis (mapping modulus plot) .

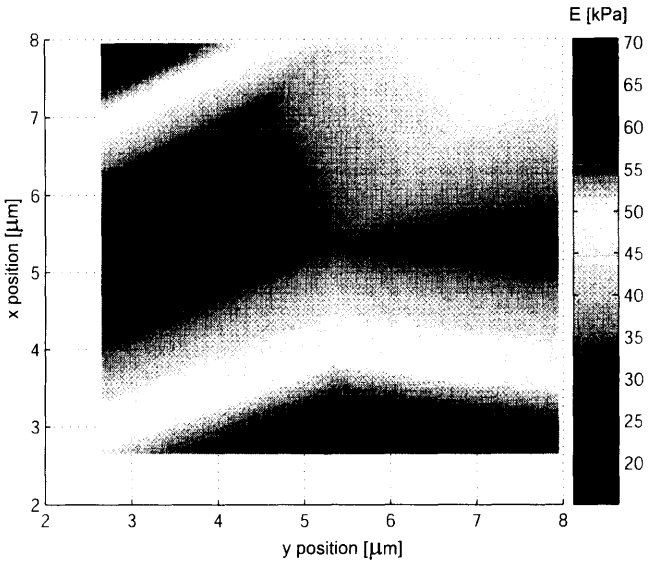

Figure 4-25: Modulus values at various points on cell for the region shown in Figure 4-24(b).

increasing is labeled as z_0. The fitting of the curve starts from this point. The Poisson's ratio is assumed to be 0.5. Even though this value will differ based on the point of indentation, it is impossible to extract the Poisson's ratio independent of E. The modulus of the points were in the kPa range, which is close to the values reported in the literature [51]. Figure 4-25 shows E for the points shown in figure 4-24b.

Discussion

Modulus mapping of deformable polymeric films is a very good technique to extract local mechanical properties. However, these properties are largely dependent on the type of indenter geometry used for indentation, as well as the depth to which the indentation is made. For example, the thinner regions of the cell give a modulus value of E higher than the actual value because of the finite thickness effects which were discussed in detail in section 4.1.1. To accommodate this problem, lower forces should be used for indentation [12]. The overprediction of E for polymeric films, due to the choice of larger range of forces are shown in detail by Domke et al [12].

Another problem specifically encountered in this study was the lower number of

points in the data range chosen. This makes it difficult to fit the curve accurately. This could be solved by increasing the number of points for the entire force-deflection map. Regardless of these problems, the force-volume technique provides a means and method to directly measure the elastic modulus of cells, which can subsequently be used as a powerful tool for analyzing living cell moduli as a result of changes in external environment.

Chapter 5

Conclusions and Future Work

The systematic computational evaluation of contact-enabled mechanical characterization of nano-scale thin film brings out several key features. In order to determine E of these thin films, the effect of finite thickness and non-linear elastic deformation should be included. The inclusion of these effects enables classical formulations derived for deformable contact bodies to be used to successfully and efficiently to extract the E. Even when the strain fields exceed the nominal elastic values, the magnitude of E does not exceed by an order of two. Also, the choice of larger indenter radii R should be made with caution, because the manner in which stress fields evolve inside the region of indenter-substrate contact during indentation changes significantly with R, hence influencing the calculated E.

There is not significant difference in estimations of E when the angle of indentation θ is varied from 0° to 15° for $h_{max} \approx R$. The effects that dominate during the indentation on nanoscale films are that of thickness rather than angle of indentation. This means that the factor that dominates the thin film indentation are the geometric effects. While using these thin films are synthetic substrates for analyzing cellular functions it is seen that the effects of displacement field felt towards normal to the focal adhesion are more dominant compared to the component along the substrate. The effects of modulus variations are pronounced normal to the cellular traction and towards the thickness of the substrate in comparison to the surface. This might mean that the cellular strains exerted during cellular functions are felt more on the extra-

cellular matrix or on cells that are directly below the point of exertion of tractive forces compared to cells that are adhered directly to the substrate.

The modulus mapping could be developed as a useful tool to analyze cellular and substrate mechanical properties. These in turn would provide crucial clues to the working of cell when its mechanical and chemical enviroment are varied.

The future work will be aimed at identifying how the bidirectional relations between cell and its local microenvironment vary at points of contact between cell and the substrate. This would involve methods such as modifying the stiffness of the underlying substrate, varying the chemical environment surrounding the cells and looking at how these changes affect cellular mechanotransductions, using computational methods.

Bibliography

[1] Nathalie Q. Balaban; Ulrich S. Schwarz; Daniel Riveline; Polina Goichberg; Gila Tzur; Ilana Sabanay; Diana Mahalu; Sam Safran; Alexander Bershadsky; Lia Addadi and Benjamin Geiger. Force and focal adhesion assembly: a close relationship studied using elastic micropatterned substrates. *Nature cell biology*, 3(5):466–472, 2001.

[2] Green A.E. and Zerna W. *Theoretical Elasticity.* Oxford Clarendon Press, 1968.

[3] Nathalie Q. Balaban Alexander D. Bershadsky, Geiger, and Benjamin. Adhesion-dependent cell mechanosensitivity. *Annu. Rev. Cell Dev. Biol.*, 19:677–695, 2003.

[4] Taylor J. Ashley. The mechanical properties and microstructure of plasma enhanced chemical vapor deposited silicon nitride thin films. *Journal of Vacuum Science and Technology A: Vacuum, Surfaces, and Films*, 9(4):2464–2468, 1991.

[5] N. Almqvist; R. Bhatia; G. Primbs; N. Desai; S. Banerjee and R. Lal. Elasticity and adhesion force mapping reveals real-time clustering of growth factor receptors and associated changes in local cellular rheological properties. *Biophys. J.*, 86:1753–1762, 2004.

[6] Emilios K Dimitriadis; Ferenc Horkay; Julia Maresca; Bechara Kachar; Richard S Chadwick. Determination of elastic moduli of thin layers of soft material using the atomic force microscope. *Biophysical Journal*, 82(5):2798–2810, May 2002.

[7] Ken Jacobson Christian Rotsch and Manfred Radmacher. Dimensional and mechanical dynamics of active and stable edges in motile fibroblasts investigated by using atomic force microscopy. *PNAS*, 96:921–926, 1999.

[8] M Radmacher; M Fritz; CM Kacher; JP Cleveland and PK Hansma. Measuring the viscoelastic properties of human platelets with the atomic force microscope. *Biophys. J.*, 70:556–567, 1996.

[9] Lei Zhai; Adam J. Nolte; Robert E. Cohen and Michael F. Rubner. ph-gated porosity transitions of polyelectrolyte multilayers in confined geometries and their application as tunable bragg reflectors. *Macromolecules*, 37(16):6113–6123, 2004.

[10] Yin FCP Costa KD. Analysis of indentation: Implications for measuring mechanical properties with atomic force microscopy. *Journal of biomechanical engineering - Transactions of the ASME*, 121(5):462–471, OCT 1999.

[11] M. F. Doerner and W. D. Nix. A method for interpreting the data from depth-sensing indentation instruments. *Journal of Materials Research*, 1(4):601, 1986.

[12] J. Domke and M. Radmacher. Measuring the elastic properties of thin polymer films with the atomic force microscope. *Langmuir*, 14:3320–3325, 1998.

[13] Jan Domke and Manfred Radmacher. The elastic indentation of thin films - a parametric model for the application in atomic force microscopy part ii: Experiments. *unpublished*, 2002.

[14] Berg M. C.; Yang S. Y.; Hammond P. T.; Rubner M. F.;. Controlling mammalian cell interactions on patterned polyelectrolyte multilayer surfaces. *Langmuir*, 20(4):1362–1368, 2004.

[15] M Radmacher; M Fritz and PK Hansma. Imaging soft samples with the atomic force microscope: gelatin in water and propanol. *Biophys. J.*, 69:264–270, 1995.

[16] Roger D. Kamm Hayden Huang and Richard T. Lee. Cell mechanics and mechanotransduction: pathways, probes, and physiology. *Am J Physiol Cell Physiol*, 287:C1–C11, 2004.

[17] J. Reine Angew Hertz H. *Mathematik*, pages 156–171, 1882.

[18] Wei hui Guo; Margo T. Frey; Nancy A. Burnham and Yu li Wang. Substrate rigidity regulates the formation and maintenance of tissues. *Biophysical Journal*, 90:2213–2220, 2006.

[19] Jeffrey L. Hutter. Comment on tilt of atomic force microscope cantilevers: Effect on spring constant and adhesion measurements. *Langmuir*, 21:2630–2632, 2005.

[20] Mendelsohn J. D.; Yang S. Y.; Hiller J.; Hochbaum A. I. and Rubner M. F.;. Rational design of cytophilic and cytophobic polyelectrolyte multilayer thin films. *Biomacromolecules*, 4(1):96–106, 2003.

[21] Mahaffy R. E.;Park S.;Gerde E.;Kas J. and Shih C.K. Quantitative analysis of the viscoelastic properties of thin regions of fibroblasts using atomic force microscopy. *Biophysical Journal*, 86(3):1777–1793, 2004.

[22] Tsui T.Y. ; Vlassak J. and Nix W.D. Indentation plastic displacement field: Part i. the case of soft films on hard substrates. *Journal of Materials Science*, 14(6):2196–2203, 1999.

[23] W. K. Wan; S. Uniyal;M. Leabu J. L. Hutter; J. Chen and B. M. C. Chan. Atomic force microscopy investigation of the dependence of cellular elastic moduli on glutaraldehyde fixation. *Journal of Microscopy*, 219:61–68, 2005.

[24] Dennis E. Discher; Paul Janmey and Yu li Wang. Tissue cells feel and respond to the stiffness of their substrate. *Science*, 310:1139–1143, 2005.

[25] Lars-Oliver Heim; Michael Kappl and Hans-Jurgen Butt. Tilt of atomic force microscope cantilevers: Effect on spring constant and adhesion measurements. *Langmuir*, 20:2760–2764, 2004.

[26] Van Vliet KJ. *Nanomechanics of crystalline materials:experiments and computations.* PhD thesis, Massachusetts Institute of Technology, 2002.

[27] Markus Preuss Lars-Oliver Heim, Jurgen Blum and Hans-Jrgen Butt. Adhesion and friction forces between spherical micrometer-sized particles. *Physical Review letters*, 88:3328–3331, 1999.

[28] Chen C.S. Liu, W.F. Engineering biomaterials to control cell function. *Materials Today*, 12(8):28–35, 2005.

[29] Karcher H et al. Mack PJ, Kaazempur-Mofrad MR. Force-induced focal adhesion translocation: effects of force amplitude and frequency. *American journal of physiology - Cell Physiology*, 287(4):C954–C962, 2004.

[30] Jrme M. Goffin; Philippe Pittet; Gabor Csucs; Jost W. Lussi; Jean-Jacques Meister and Boris Hinz. Focal adhesion size controls tension-dependent recruitment of alpha-smooth muscle actin to stress fibers. *Journal of Cell Biology*, 172:259–268, 2006.

[31] M. Mooney. A theory of large elastic deformation. *Journal of Applied Physics*, 11(9):582–592, 1940.

[32] Ranjana Saha Nix and William D. Effects of the substrate on the determination of thin film mechanical properties by nanoindentation. *Acta Materialia*, 50(1):23–38, 2002.

[33] Ulrich G. Hofmann; Christian Rotsch; Wolfgang J. Parak and Manfred Radmacher. Investigating the cytoskeleton of chicken cardiocytes with the atomic force microscope. *Journal of Structural Biology*, 119(2):84–91, 1997.

[34] DE Laney; RA Garcia; SM Parsons and HG Hansma. Changes in the elastic properties of cholinergic synaptic vesicles as measured by atomic force microscopy. *Biophys. J.*, 72:806–813, 1997.

[35] R. J. Pelham and Y. L. Wang. Cell locomotion and focal adhesions are regulated by substrate flexibility. *Proceedings Of The National Academy Of Sciences Of The United States Of America*, 94(25):13661–13665, 1997.

[36] W. C. Oliver; G. M. Pharr. An improved technique for determining hardness and elastic modulus using load and displacement sensing indentation experiments. *Journal of Materials Research*, 7(6):1564, 1992.

[37] Adam J. Engler;Ludovic Richert; Joyce Y. Wong; Catherine Picart and Dennis E. Discher. Surface probe measurements of the elasticity of sectioned tissue, thin gels and polyelectrolyte multilayer films: Correlations between substrate stiffness and cell adhesion. *Surface Science*, 570(1-2):142–154, 2004.

[38] Pethica J.B.;Hutchings R and Oliver W.C. Hardness measurement at penetration depths as small as 20-nm. *Philosophical Magazine A-Physics of condensed matter structure defects and mechanical properties*, 48(4):593–606, 1983.

[39] Christian Rotsch and Manfred Radmacher. Drug-induced changes of cytoskeletal structure and mechanics in fibroblasts: An atomic force microscopy study. *Biophys. J.*, 78:520–535, 2000.

[40] Michael T. Thompson; Michael C. Berg; Irene S. Tobias; Michael F. Rubner and Krystyn J. Van Vliet. Tuning compliance of nanoscale polyelectrolyte multilayers to modulate cell adhesion. *Biomaterials*, 26(34):6836–6845, 2005.

[41] Amy Shaub. Unravelling the extracellular matrix. *Nature cell biology*, 1(November):E173–E175, 1999.

[42] Ian N. Sneddon. The relation between load and penetration in the axisymmetric boussinesq problem for a punch of arbitrary profile. *International Journal of Engineering Science*, 3(1):47–57, 1965.

[43] ABAQUS /Standard. 2005.

[44] Chen W. T. and P.A. Engel. Impact and contact stress analysis in multilayer media. *Int. J Solids Struct.*, 8:1257–1281, 1972.

[45] D. Tabor. *The Hardness of Metals.* Oxford: Clarendon Press, 1951.

[46] Kim Min Tae. Influence of substrates on the elastic reaction of films for the microindentation tests. *Thin Solid Films*, 283:12–16, 1996.

[47] Alexander D. Bershadsky Tom Shemesh, Benjamin Geiger and Michael M. Kozlov. Focal adhesions as mechanosensors: A physical mechanism. *PNAS*, 102(35):12383–12388, 2005.

[48] TRUEGRID v 2.2.3. 2005.

[49] Micah Dembo Wang and Yu-Li. Stresses at the cell-to-substrate interface during locomotion of fibroblasts. *Biophysical Journal*, 76:2307–2316, 1999.

[50] Tony Yeung; Penelope C. Georges; Lisa A. Flanagan; Beatrice Marg; Miguelina Ortiz; Makoto Funaki; Nastaran Zahir; Wenyu Ming; Valerie Weaver and Paul A. Janmey. Effects of substrate stiffness on cell morphology, cytoskeletal structure, and adhesion. *Cell Motility and the Cytoskeleton*, 60(1):24–34, 2005.

[51] Christian Rotsch; Filip Braet; Eddie Wisse and Manfred Radmacher. Afm imaging and elasticity measurements on living rat liver macrophages. *Cell Biology International*, 21(11):685–696, 1997.

[52] Chen W.T. Computation of stresses and displacements in a layered elastic medium. *Int. J. Eng Sci.*, 9:775–800, 1971.

[53] Hong Xing You; Joan M. Lau; Shengwen Zhang and Lei Yu. Atomic force microscopy imaging of living cells: a preliminary study of the disruptive effect of the cantilever tip on cell morphology. *Ultramicroscopy*, 82:297–305, 2000.